A W-Band Dual-Polarization Slot Array Antenna with Low Sidelobe Level

Hao Luo [1], Yu Xiao [2], Wenhao Tan [1], Luoning Gan [1], and Houjun Sun [1]

[1] Department of Information and Electric Engineering
Beijing Institute of Technology, Beijing, 100081, China
ihlyt111@126.com

[2] Department of Electronic Engineering
Tsinghua University, Beijing, 100081, China
xiaoyummw@tsinghua.edu.cn

Abstract ─ A 94-GHz dual-polarization low-sidelobe-level slot array antenna is proposed. A 2x2-slot cavity-backed subarray is adopted as the basic unit of the array. A high-isolation orthogonal-mode transducer (OMT) with a simple structure is used to excite the dual-polarization subarray. The realization of a low sidelobe level depends on the amplitude-weighted waveguide feed network. A novel unequal power dividing ratio but equal phase (UPEP) single-ridged waveguide divider is presented for the construction of the vertical polarization (VP) array feed network. A 16x16-slot low-sidelobe-level dual-polarization array antenna is fabricated. The machining difficulties of the W-band array are reduced by using simpler structures. The measured results show that the impedance bandwidth is greater than 7.3 GHz, while the first sidelobe levels are lower than -20.1 dB for both polarization arrays within the operating bandwidth. The measured gain is higher than 30.9 dBi for the two polarization arrays with an antenna efficiency better than 64% .

Index Terms ─ Dual-polarization, low sidelobe level, slot array antenna, *W*-band.

I. INTRODUCTION

Fully polarimetric radar has advantages in anti-interference properties and has received increasing attention in recent years. The dual-polarization antenna is the key part of achieving the polarization agility of a fully polarimetric radar system [1]. The reported dual-polarization reflector antenna and lens antenna have a high gain but suffer from a high profile [2-3].

Most reported dual-polarization planar antennas are based on dielectric substrates because of their low profile and low cost [4-9]. Microstrip patch antennas were used as the dual-polarization radiating elements in [5-8]. High isolation between the two polarization arrays has been achieved by multilayer feed networks; however, these antennas have a low radiation efficiency due to the large loss of the microstrip feed network. In [8-9], a substrate-integrated waveguide feed network was used, and the antenna efficiency increased but remained at a low level because the dielectric loss could not be ignored, especially in the millimeter-wave band.

Waveguide slot antennas employ a low-loss feed network, leading to an easier realization of a low sidelobe level, which has been widely used in the millimeter wave band [10-12]. However, these slot arrays are actually series-fed, which results in a narrow bandwidth due to the long-line effect.

The basic units of the cavity-backed slot antennas in [13-17] use the resonance mode in the cavity to feed the slots instead of a conventional feed network, which results in lower feeding loss and wider bandwidth. In addition, corporate feed networks are adopted in cavity-backed slot arrays, resulting in high-gain and wideband performance. Due to the good performance, a large number of cavity-backed slot array antennas with different radiating elements, different transmission lines and different frequencies have been studied and reported [13-21]. Few of these studies have mentioned low-sidelobe-level design in a dual-polarization array, however, for radar systems, low-sidelobe-level antennas can improve the anti-jamming ability of the system.

The goal of this paper is to present a method to design the wideband high-gain dual-polarization slot array antenna with a low-sidelobe-level design in the W-band. First, we introduce the basic unit of the dual-polarization array and analyze the working mechanism of the orthogonal-polarization feeding structure. Next, we introduce the design of the unequal power dividing ratio but equal phase single-ridge waveguide divider in detail. Finally, a 16x16-slot dual-polarization array with a low sidelobe level is fabricated and measured to verify the design method.

II. ANTENNA DESIGN

The total structure of the proposed W-band dual-

Submitted On: May 23, 2019
Accepted On: July 19, 2019

polarization 16x16-slot cavity-backed array antenna is shown in Fig. 1. The antenna consists of six metal layers. The upper two layers are the radiating part of the array, and the third and fifth layers are the 1-to-64-way amplitude-weighted feed networks of the vertical polarization and horizontal polarization arrays. The power-weighted feed-networks are composed of the UPEP rectangular waveguide dividers and UPEP single-ridge waveguide dividers. The isolation bars and coupling windows are in the fourth layer, and they are the key to realizing high isolation between the feed networks of the two polarization arrays. The sixth layer is the backboard, and two WR-10 standard waveguides with an FUGP-385 flange are used as the feeding ports.

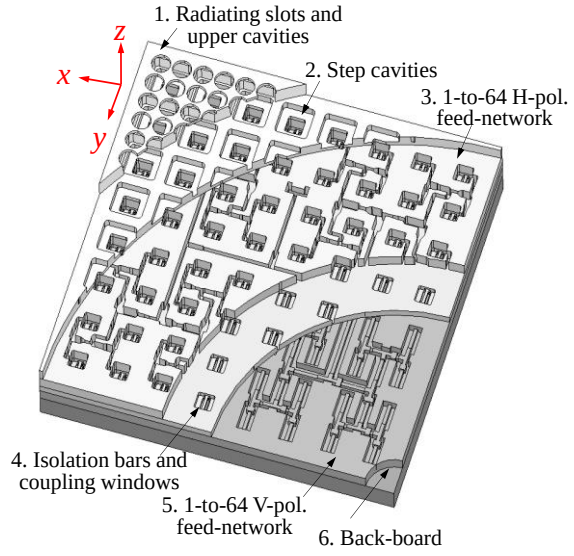

Fig. 1. Configuration of the dual-polarization array.

A. The dual-polarization cavity-backed slot subarray

As shown in Fig. 2, the basic unit of the array is a cavity-backed 2x2-slot subarray. Circular radiating slots and square cavities with large fillets are used instead of the narrow slots and irregularly shaped cavities in [13] to reduce the machining difficulties in the W-band. The radiating slots and the upper cavity have a rotationally symmetrical structure that can radiate uniformly for both polarizations. The radiating part is fed by a square waveguide, and a step cavity is adopted to improve the impedance bandwidth of the feed waveguide. The horizontal-polarization (HP) electromagnetic (EM) wave is fed from an E-plane rectangular waveguide through the z-direction coupling window etched on the sidewall of the square waveguide, and the VP EM wave is fed by a single-ridged waveguide through the y-direction coupling window on the bottom of the square waveguide.

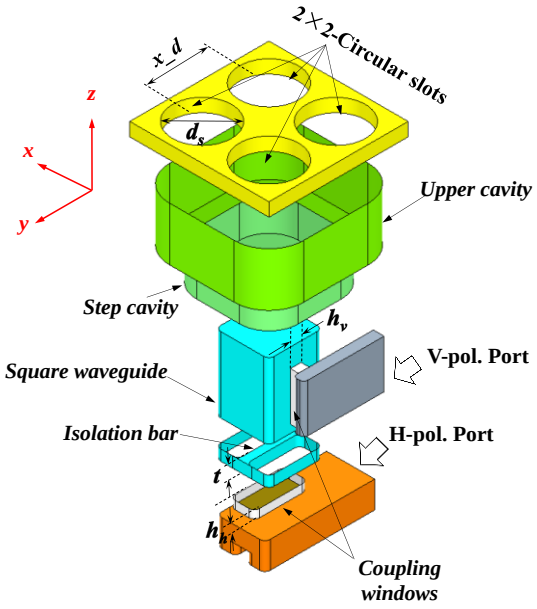

Fig. 2. Configuration of the basic unit in the array.

As shown in Fig. 3, the isolation bar can cut off the HP EM wave, while the z-direction coupling slot can cut off the VP EM wave, the isolation between the two ports can be estimated by formula (1):

$$I_s = 20\log_{10} e^{\alpha L}, \tag{1}$$

where α is the attenuation constant of TE_{10} mode, L is the sum of *hv*, h_h and *t*. As depicted in Fig. 4, the isolation between HP and VP ports is lower than -45dB among 88GHz~100GHz. Compared with the feeding structure in [21], the orthogonal-mode transducer adopted in our work has a more compact structure and a higher isolation so that the two polarization feed-networks can be designed independently.

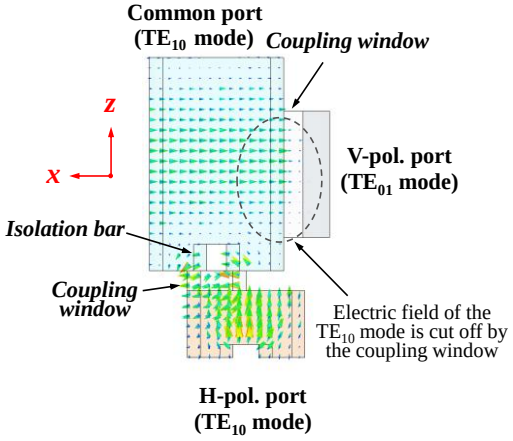

(a) Electric field distribution in the OMT (H-pol.)

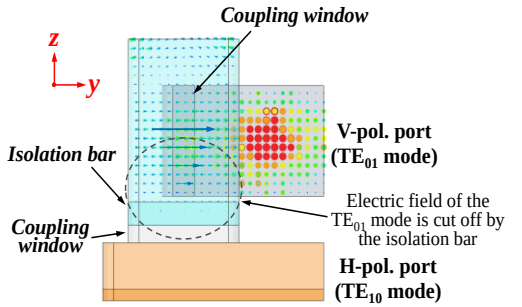

(b) Electric field distribution in the OMT (V-pol.)

Fig. 3. Working mechanism of the OMT.

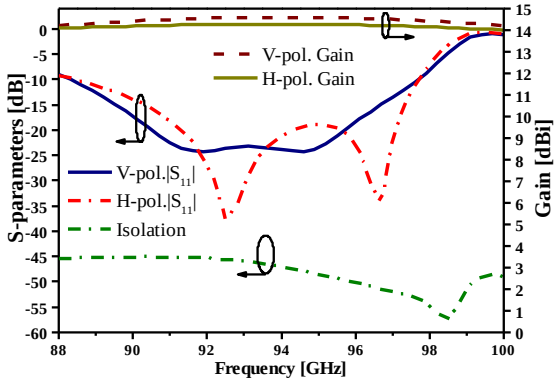

Fig. 4. Simulated performance of the subarray.

The EM simulation software Ansoft HFSS is used to analyze the performance of the antenna. The S-parameters and gain of the basic unit are depicted in Fig. 4, and the radiation patterns of the basic unit are exhibited in Fig. 5. The reflection coefficients of the VP and HP units are lower than -10 dB over the frequency range of 88.5 GHz~96.8 GHz. The simulated gain is higher than 14 dBi, and the cross-polarization discrimination (XPD) is lower than -39 dB in both planes for the two polarization units.

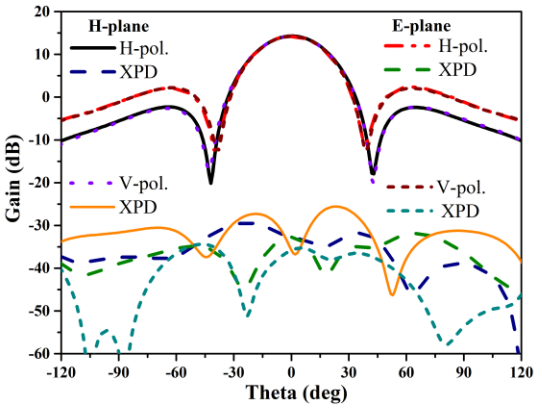

Fig. 5. Radiation pattern of the subarray (94GHz).

B. Design of the UPEP waveguide dividers

When using the 2x2-slot unit to build a wideband large-scale array, the low-sidelobe-level performance of the array antenna needs to be realized by an amplitude-weighted corporate feed network.

The UPEP waveguide divider is the basic unit of the amplitude-weighted feed network in rectangular waveguide (RWG). The characteristic impedance of Z_0 and phase constant β of the TE_{10} mode in a rectangular WG are listed in (2) and (3):

$$\beta = \frac{2\pi}{\lambda}\sqrt{1-\left(\frac{\lambda}{2a}\right)^2}, \tag{2}$$

$$Z_e = \frac{b}{a}\sqrt{\frac{\mu}{\varepsilon}}\frac{1}{\sqrt{1-(\lambda/2a)^2}}, \tag{3}$$

where a and b are the broad wall width and narrow width of an RWG. The realization of the UPEP RWG divider is through tuning the narrow wall width of RWG. This method can be used to build the VP amplitude-weighted feed network. However, a UPEP single-ridge waveguide divider should also be designed to build the HP amplitude-weighted feed network.

Unlike the RWG, the electric field and magnetic field distributions in an SRWG are more complicated. At present, there are few studies on a UPEP single-ridge waveguide divider.

The key to realizing a UPEP divider is to find a waveguide parameter that affects the characteristic impedance (Z_e) of the waveguide but has a small effect on the guide wavelength (λ_g). Figure 6 shows curves of the characteristic impedance and guide wavelength of a single-ridge waveguide with different values of the ridge width a_2; for the SRWG, when the ridge height b_2 is close to the height of the waveguide b_2, the ridge width a_2 is proportional to the characteristic impedance Z_e but independent of the guide wavelength λ_g.

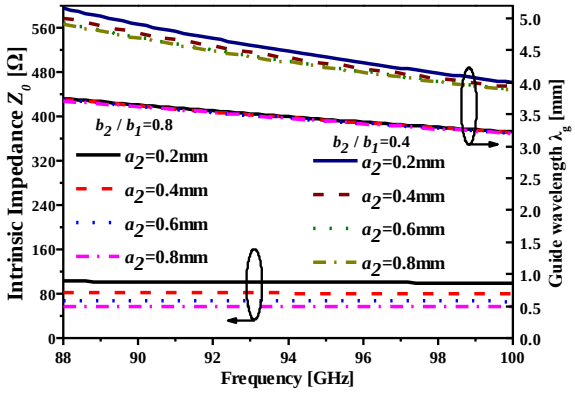

Fig. 6. Simulated results of a single-ridge waveguide.

Based on this discovery, we proposed the UPEP single-ridge waveguide divider, which is shown in Fig. 7. A power splitting SRWG section is added to both

output WGs. The ridge heights of the two SRWG sections are close to the height of the SRWG ($b_2 \approx b_1$). By adjusting the ridge width of the two SRWG sections, an unequal power dividing ratio but equal phase can be achieved. An impedance matching section is placed at the input port to broaden the bandwidth. The impedance of this section can be calculated by formula (4):

$$Z_1 = \sqrt{Z_0 Z_2 Z_3 (Z_2 + Z_3)}. \quad (4)$$

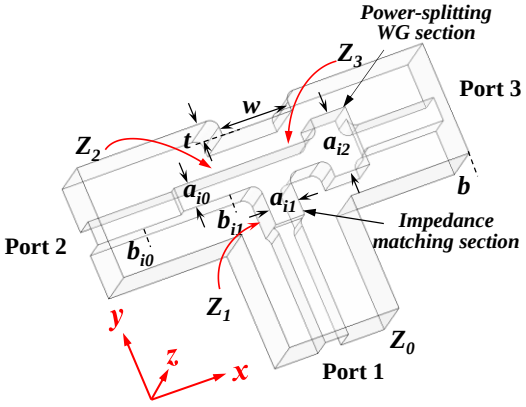

Fig. 7. The proposed UPEP single-ridge waveguide divider.

Figure 8 shows the performance of the designed UPEP single-ridge waveguide divider. The power dividing ratio is 3.5 dB, and the absolute value of the phase deviations is less than 5 degrees between the two output ports, while the reflection coefficient is less than -18 dB in the frequency range of 88 GHz~100 GHz.

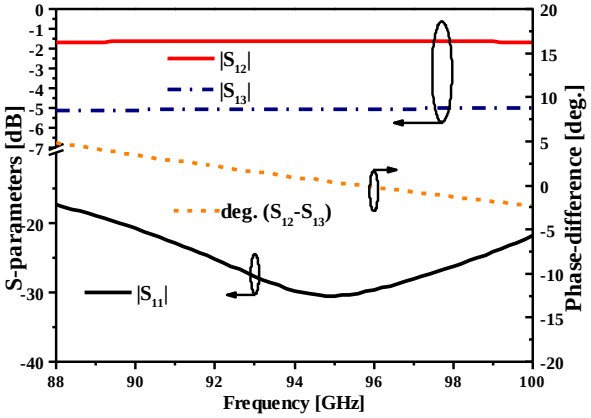

Fig. 8. S-parameters of the proposed UPEP divider.

C. Design of the amplitude-weighted feed-network

To realize the low sidelobe level of a large-scale array, we used the 2x2-slot dual-polarization subarray to build a 16x16-slot array. Two kinds of 1-to-64-way amplitude-weighted waveguide feed networks are designed in this section.

Based on the proposed UPEP single-ridge waveguide divider, a 1-to-64-way amplitude-weighted corporate feed network is built for the HP array. The amplitude-weighted feed network for the VP array consists of the UPEP rectangular waveguide divider proposed in previous work. Figure 9 shows the configuration of the H feed networks. A 25 dB Taylor synthesis is used to obtain the normalized amplitude coefficient of each output port in the two feed-networks.

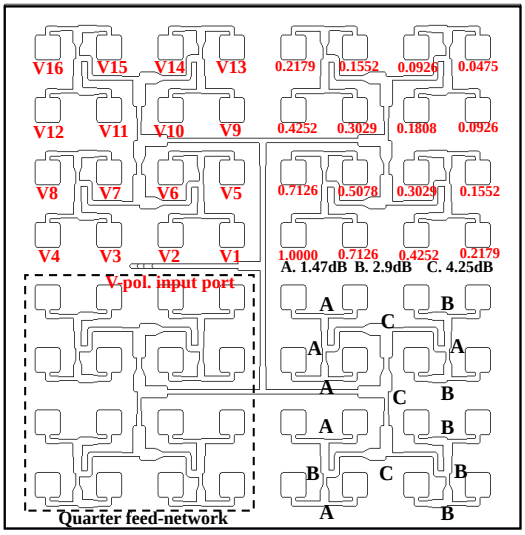

(a) Configuration of the VP array feed-network

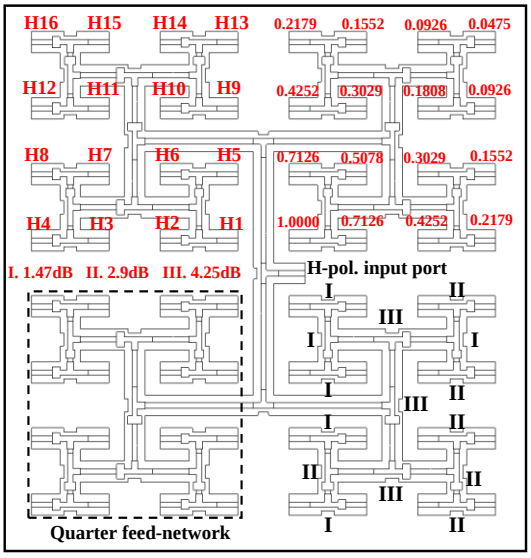

(b) Configuration of the HP array feed-network

Fig. 9. The designed amplitude-weighted feed-networks.

Three UPEP power dividers with power splitting ratios of 4.25 dB, 2.9 dB and 1.47 dB are required for each feed network. Their corresponding positions are also shown in Fig. 9.

The feed ports of the array are two WR-10 standard waveguides with an FUGP-385 flange. As shown in Fig. 10, a vertical transition from the single-ridge waveguide to the WR10 standard waveguide is introduced in the feed networks. The S-parameters of the vertical transition are shown in Fig. 11. The results indicate that the transition structure has a reflection coefficient of less than -22 dB in the frequency range of 88 to 100 GHz, a relative bandwidth of approximately 25.6%, and an insertion loss of less than 0.05 dB in the same frequency range.

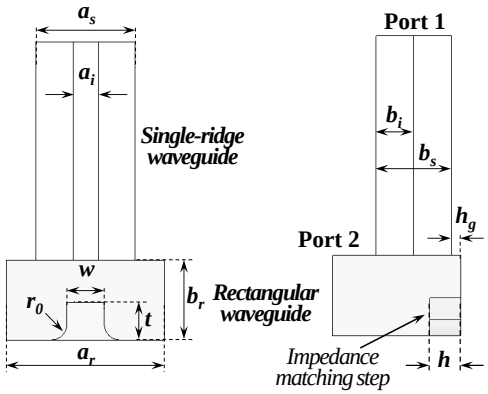

Fig. 10. Vertical transition from SRWG to RWG.

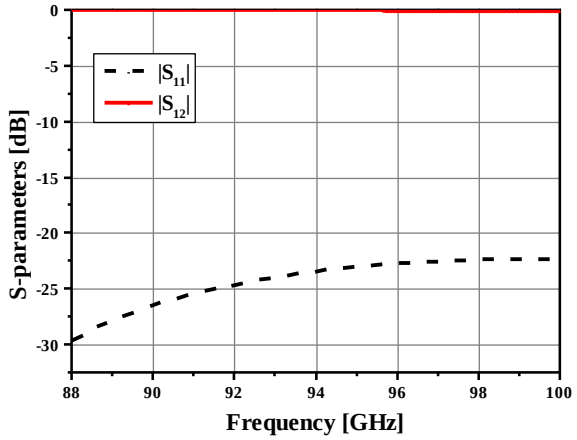

Fig. 11. Simulated performance of the vertical transition.

The simulated performance of the designed VP and HP amplitude-weighted feed networks are shown in Fig. 12. The absolute values of the phase deviation are less than 8 degrees among the 64 ports, and the absolute values of the amplitude differences are less than 0.25 dB in the frequency range of 89.2 GHz ~ 98.2 GHz. Moreover, the reflection coefficients of the HP and VP input ports are less than -10 dB from 88.5 GHz to 97.5 GHz.

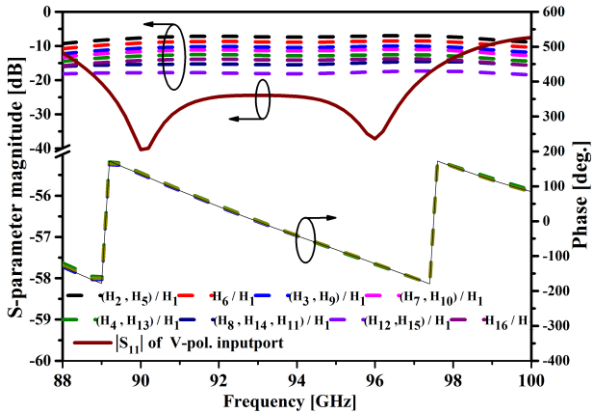

(a) Performance of the HP array feed-network

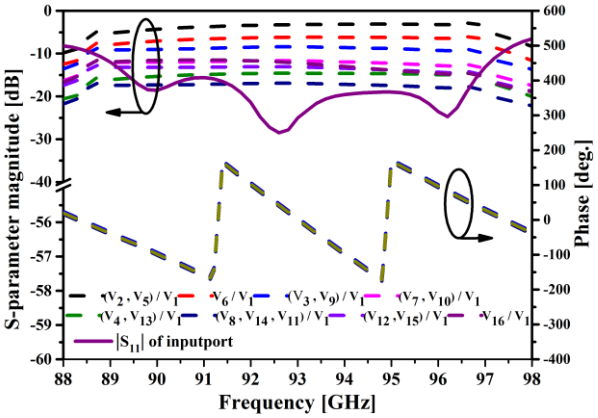

(b) Performance of the VP array feed-network

Fig. 12. Simulated results of the feed-networks.

III. MEASUREMENT AND RESULTS

The designed dual-polarization 16x16-slot cavity-backed array antenna consists of six aluminum plates and is shown in Fig. 1. These aluminum plates are machined by milling and bonded by a vacuum brazing process. The smallest milling cutter used during machining is 0.3 mm in diameter. The surface roughness inside the waveguide cavity after processing is Ra1.6. The manufacturing tolerances of the array antenna are analyzed by the HFSS software. Figure 13 shows the prototype of the proposed antenna.

The average thickness of each layer of solder after bonding is less than 0.02 mm, which is within an acceptable range. The reflection coefficient and isolation of the two polarization input ports of the array antenna were measured by the R&S ZVA-Z110 vector network analyzer. The results are shown in Fig. 14. The reflection coefficients of the HP and VP ports are less than -10 dB in the frequency range of 89.2GHz~ 96.5GHz, and the relative bandwidth is approximately 7.8%. The isolation between the two polarization feed ports is better than 45 dB in 88 GHz ~100 GHz.

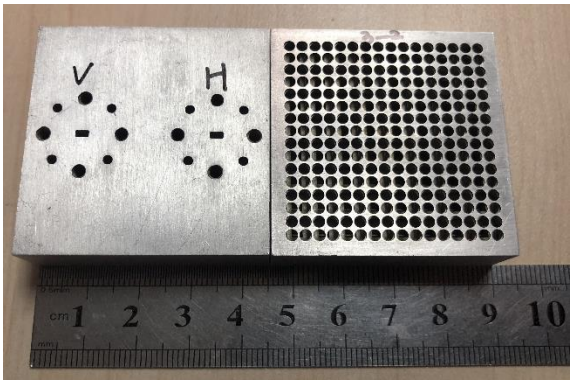

Fig. 13. Prototype of the fabricated array antenna.

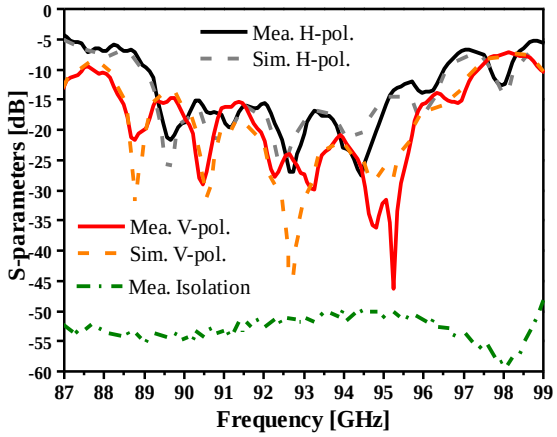

Fig. 14. Measured S-parameters of the proposed array.

The radiation performance of the dual-polarization array was measured by a W-band far-field antenna testing system in an anechoic chamber. The antenna measurement environment is shown in Fig. 15.

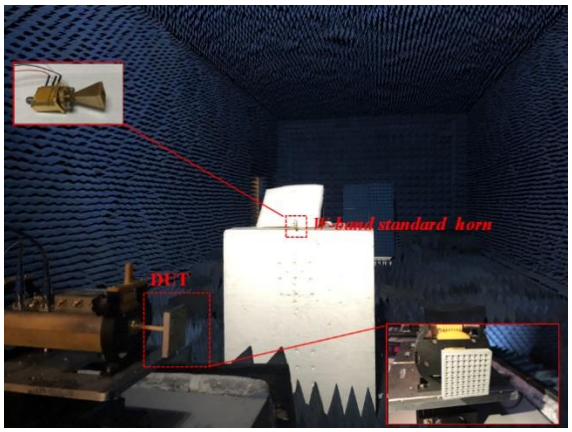

Fig. 15. Antenna measurement environment.

Figure 16 shows the measured and simulated gains of the antenna. A gain curve considering the metal loss and surface roughness is also added to the figure for a comparison. The measured gain for the VP array is higher than 31 dBi, and the measured gain for the HP array is higher than 30.9 dBi from 90 GHz to 96 GHz. The measured gain is approximately 0.6 dB lower than the simulated gain, which is caused by errors in the processing and measurement. The measured efficiency of the two polarization arrays is higher than 64% over the entire working band.

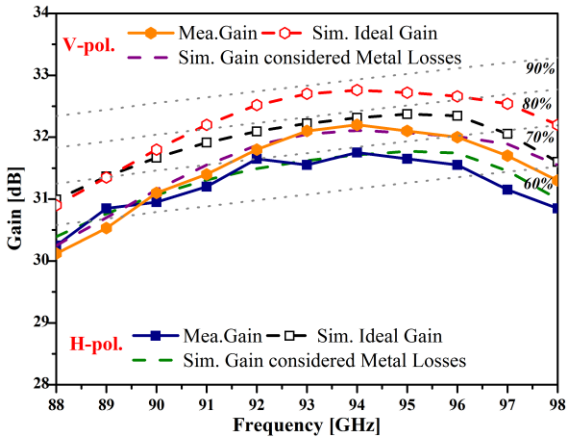

Fig. 16. Measured gain of the proposed array.

A comparison between the measured and simulated radiation patterns is shown in Fig. 17. The measured sidelobe levels for the VP and HP arrays are lower than -21 dB and -20.1 dB in both planes, respectively. The XPDs for both polarization arrays are lower than -35 dB in both planes. The measured and simulated results are highly consistent, which verifies the validity of the design method.

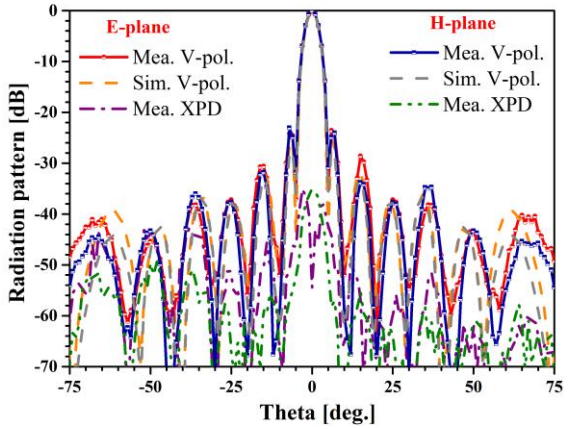

(a) Radiation pattern of the VP array (94GHz)

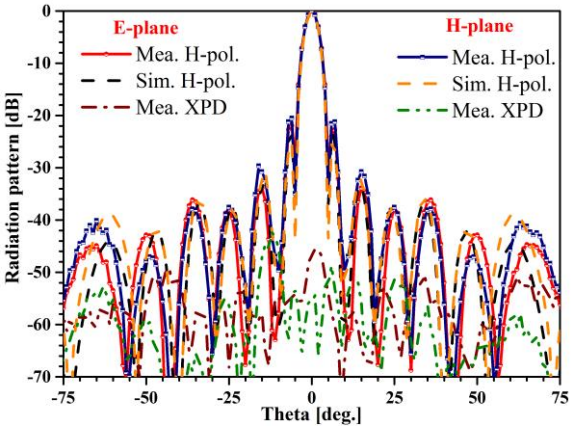

(b) Radiation pattern of the HP array (94GHz)

Fig. 17. Measured radiation pattern of the proposed array.

Table 1 presents a comparison of the antenna presented in references and our work. The performance comparison includes the center frequency, realized gain, impedance bandwidth, sidelobe-level, cross-polarization discrimination, antenna efficiency, and fabrication difficulties. The results indicate that the antenna in our work has the lowest sidelobe level with wideband and high-gain performance characteristics.

Table 1:Performance comparison of the reported planar dual-polarization antenna and our work

Ref.	**[13]**	**[19]**	**[20]**	**[21]**	**[4]**	**Our Work**
Freq. [GHz]	60	60	60	60	94	94
Gain [dB]	32.2	22.3	12.5	16.5	13.3	31.2
BW.	8%	17%	22%	15%	7%	7.8%
SLL. [dB]	-13	-12.3	-10	-13	-10	-20.1
XPD. [dB]	<-25	<-20	<-10	<-30	<-9	<-35
Effc.	80%	72%	70%	65%	50%	64%
Fabr. Diffic.	Medium	Low	Low	High	Low	Medium

IV. CONCLUSION

A 94-GHz dual-polarization low-sidelobe-level 16x16-slot cavity-backed array antenna is proposed. A high-isolation orthogonal mode transducer with a simple structure is used to excite the 2x2-circular-slot cavity-backed subarray. A new UPEP single-ridge waveguide divider is proposed for the construction of the amplitude-weighted corporate feed network. The measured first sidelobe levels are lower than -20.1 dB for both arrays from 90 GHz to 96 GHz. The measured results indicate that the fabricated W-band array antenna has wideband and high gain performance characteristics, which commendably satisfies the requirements of the W-band fully polarimetric radar system.

REFERENCES

[1] M. Andrews and P. Mitra, "Tripling the capacity of wireless communications using electromagnetic polarization," *Nature*, vol. 409, no. 1, pp. 316-318, 2001.

[2] Z. Y. Zhang, "Design of a dual-beam dual-polarized offset parabolic reflector antenna," *IEEE Trans. Antennas Propag.*, vol. 67, no. 2, pp. 712-718, 2019.

[3] Y. Su and Z. N. Chen, "A flat dual-polarized transformation-optics beamscanning luneburg lens antenna using PCB-stacked gradient index metamaterials," *IEEE Trans. Antennas Propag.*, vol. 66, no. 10, pp. 5088-5097, 2018.

[4] Z. Chen, "A 94-GHz dual-polarized microstrip mesh array antenna in LTCC technology," *IEEE Antennas Wireless Propag. Lett.*, vol. 14, pp. 1279-1281, 2015.

[5] C. L. Deng, "A high-isolation dual-polarization patch antenna with omnidirectional radiation patterns," *IEEE Antennas Wireless Propag. Lett.*, vol. 11, pp. 1273-1276, 2012.

[6] D. Sun, "Design of broadband dual-polarized patch antenna with backed square annular cavity," *IEEE Trans. Antennas Propag.*, vol. 64, no. 1, pp. 43-52, 2016.

[7] Y. Yu and W. Hong, "E-band low-profile, wideband 45° linearly polarized slot-loaded patch and its array for millimeter-wave communications," *IEEE Trans. Antennas Propag.*, vol. 66, no. 8, pp. 4364-4369, 2018.

[8] L. Wang and Y. J. Chen, "Wideband and dual-band high-gain substrate integrated antenna array for E-band multi-gigahertz capacity wireless communication systems," *IEEE Trans. Antennas Propag.*, vol. 62, no. 9, pp. 4602-4611, 2014.

[9] Y. J. Chen, "94 GHz substrate integrated waveguide dual-circular-polarization shared-aperture parallel-plate long-slot array antenna with low sidelobe level," *IEEE Trans. Antennas Propag.*, vol. 65, no. 11, pp. 5855-5861, 2017.

[10] H. Luo, "Design of a dual-polarization single-ridged waveguide slot array with enhanced bandwidth," *IEEE Antennas Wireless Propag. Lett.*, vol. 18, pp. 138-142, 2019.

[11] T. Li, "Design and implementation of dual-frequency dual-polarization slotted waveguide antenna array for Ka-band application," *IEEE Antennas Wireless Propag. Lett.*, vol. 13, pp. 1317-

1320, 2014.

[12] R. V. Gatti and R. Rossi, "A dual-polarization slotted waveguide array antenna with polarization-tracking capability and reduced sidelobe level," *IEEE Trans. Antennas Propag.*, vol. 64, no. 4, pp. 1567-1572, 2016.

[13] D. Kim, M. Zhang, J. Hirokawa, and M. Ando, "Design and fabrication of a dual-polarization waveguide slot array antenna with high isolation and high antenna efficiency for the 60 GHz band," *IEEE Trans. Antennas Propag.*, vol. 62, no. 6, pp. 3019-3027, 2014.

[14] A. Vosoogh and P. S. Kildal, "Corporate-fed planar 60-GHz slot array made of three unconnected metal layers using AMC pin surface for the gap waveguide," *IEEE Antennas Wireless Propag. Lett.*, vol. 15, pp. 1938-1935, 2016.

[15] D. Zarifi and P. S. Kildal, "Design and fabrication of a high-gain 60-GHz corrugated slot antenna array with ridge gap waveguide distribution layer," *IEEE Trans. Antennas Propag.*, vol. 64, no. 7, pp. 2905-2913, 2016.

[16] B. L. Cao, "W-band high-gain TE_{220}-mode slot antenna array with gap waveguide feeding network," *IEEE Antennas Wireless Propag. Lett.*, vol. 15, pp. 988-991, 2016.

[17] Y. J. Chen, "W-band large-scale high-gain planar integrated antenna array," *IEEE Trans. Antennas Propag.*, vol. 62, no. 6, pp. 3370-3373, 2014.

[18] Z. J. Chen, "High gain, broadband and dual-polarized substrate integrated waveguide cavity-backed slot antenna array for 60 GHz band," *IEEE Access.*, vol. 6, pp. 31012-31022, 2018.

[19] Y. J. Li and K. M. Luk, "60-GHz dual-polarized two-dimensional switch-beam wideband antenna array of aperture-coupled magneto-electric dipoles," *IEEE Trans. Antennas Propag.*, vol. 64, no. 2, pp. 554-563, 2016.

[20] M. F. Rocher and A. V. Nogueira, "A dual-polarized slotted-waveguide antenna based on gap waveguide technology," *11th European Conf. on Antennas and Propagat. (EUCAP)*, 19-24 March 2017.

[21] A. Jawad, T. Djerafi, and K. Wu, "A 94-GHz planar orthogonal mode transducer," *International Journal of Microwace and Wireless Tech.*, vol. 6, no. 3, pp. 313-324, 2014.

Hao Luo was born in Yunnan Province, P. R. China in 1990. He received the B. S. degree in Electrical Engineering from Beijing Institute of Technology in 2012. He received the M. S. degree in Electrical Engineering from Beijing Institute of Technology in 2015. He began his PhD degree in 2015 and his interest field is mainly in millimeter wave antenna, dual-polarization antenna, and full-polarimetric radar systems.

Yu Xiao received his Ph.D. degree in Electrical Engineering from Beijing Institute of Technology in 2017. He is now a Post-Doctor in Tsinghua University, his interest field is mainly in millimeter wave system, plannaer antennas.

Wenhao Tan was born in Anhui, China, in 1995. He received the B.S. degree in Electronic and Information Engineering from Beijing Institute of Technology, Beijing, China, in 2017. He is currently pursuing the M. Eng. degree in Electromagnetic Fields and Microwave Technology at Beijing Institute of Technology, Beijing, China. His current research interests include millimeter wave antenna and silicon antenna.

Luoning Gan was born in Liaoning, China, in 1994. He received the B.S. degree in Applied Physics from Beijing Institute of Technology, Beijing, China, in 2016. He is currently pursuing the M. Eng. degree in Electromagnetic Fields and Microwave Technology in Beijing Institute of Technology, Beijing, China. His current research interests include microwave and millimeter wave antennas.

Houjun Sun received his Ph.D. degree in Communication and Electronic Systems from BIT in 1997. He is currently a Professor in BIT, the Director of the Institute of Microwave Technology, and the Director of the Beijing Key Laboratory of Millimeter Wave and Terahertz Technology. His current research interests include the integration and application of the millimeter-wave and terahertz communication system, active antenna arrays, millimeter-wave imaging.